Road Profile Estimation and Preview Control For Low-Bandwidth Active Suspension Systems

Christoph Göhrle, Andreas Schindler, Andreas Wagner, and Oliver Sawodny

Abstract—**Active suspensions in vehicles can apply a vertical force between the wheel and the vehicle body in order to reduce vehicle body motion over road obstacles, enhancing ride comfort. In this study, new methods are developed to generate a preview road height profile using vehicle sensors and to control the active suspension using this information. To control the actuators, two concepts are developed: a feedforward disturbance compensation, calculated from the preview signal, combined with a feedback loop without preview and a preview model predictive control approach. After defining a desired road height profile as input for the designed control algorithms, a sensor-fixed and an inertial coordinate system to compile the road height profile from sensor measurements are proposed. Methods to transform the sensor data from one time step to another, to accumulate redundant measurements, and a filtering technique to shape the road signal are developed. To test the algorithms, a simulation from the road signal generation to the suspension control is designed, and additionally, an observer is derived to determine the road height profile from vehicle motion in order to verify the preview signal. Simulation results and measurements of vehicle implementation are presented.**

Index Terms—**Active suspension, filtering, predictive control, preview control, road profile.**

I. INTRODUCTION

SINCE the beginning of car manufacturing, the improvement of ride comfort and handling characteristics has been an important ambition of automotive companies. In addition, there are constantly more sophisticated sensors, which detect the surroundings of the car, in modern vehicles, to support the driver with advanced driver assistance systems. These sensors can also be used to detect the road height profile in front of the car for improved control of active suspension systems. The main goal of an active suspension is to improve ride comfort, which is measured by a reduction of vehicle body accelerations.

First, the state of the art for active suspension systems without preview is briefly summarized. In the current literature, a large variety of controller design schemes, e.g., a linear-quadratic regulator (LQR) [1]–[3], H_∞-control [4]–[8], robust control [9], and model predictive control (MPC) without preview [10]–[12], based on a quarter-car, a half-car, and a full-car model are applied for suspension systems. The most common approach,

also used in series-production vehicles with semiactive suspensions, is the so-called *Skyhook* control [13]. Applied to a full-car model, this approach calculates a desired vertical force of the vehicle body $F_{z,\text{des}}$, a desired pitch momentum $T_{\varphi,\text{des}}$, and a desired roll momentum $T_{\theta,\text{des}}$ as if the vehicle body is damped by a virtual damper to the sky

$$\begin{pmatrix} F_{z,\text{des}} \\ T_{\varphi,\text{des}} \\ T_{\theta,\text{des}} \end{pmatrix} = \begin{pmatrix} -b_z & 0 & 0 \\ 0 & -b_\varphi & 0 \\ 0 & 0 & -b_\theta \end{pmatrix} \begin{pmatrix} \dot{z}_{b,\text{filt}} \\ \dot{\varphi}_{\text{filt}} \\ \dot{\theta}_{\text{filt}} \end{pmatrix}. \quad (1)$$

The pitch rate $\dot{\varphi}$ and the roll rate $\dot{\theta}$ are measurement signals in modern vehicles and need to be low-pass filtered, the heave velocity $\dot{z}_b$ is calculated by high-pass filtering, integration, and low-pass filtering of the vertical acceleration, which is also a measurement signal. The parameters b_z, b_φ, and b_θ need to be adapted for good ride comfort, and the actuator forces at each wheel are calculated from the desired force and momenta with regard to the wheel base and track width of the vehicle.

Furthermore, different concepts for preview suspension control are proposed, based on the assumption that a vehicle sensor measures the road height in a specific range in front of the car. The time delay from the measurement until the vehicle drives over that road segment is compensated for using a Padé approximant and a LQR is applied [14]–[18]. Another approach is to augment the state space to compensate for the time delay by shifting the measured height value in the augmented state space until it affects the system [19]–[23]. The Padé approximant implies imprecision, and the augmented state space formulation is only valid for a particular speed. In this study, a discrete shift register, as in [24], is used, so that the corresponding height values are available for the controller and the compensation of the delay from measuring the road in front of the car until it affects the vehicle does not need to be incorporated in controller design.

An optimal control for previewing active suspension systems can be derived using the Hamilton function [25]–[27]. This is the common approach in the current literature [28]–[37] and results in a LQR as a state feedback and a preview feedforward term calculated from the oncoming road height profile. Furthermore, MPC is a promising design scheme [38]–[42], since information about the future is available and actuator constraints can be explicitly incorporated.

In [43], the authors investigated different MPC approaches for a given optimal road height profile and showed the effectiveness of the controllers in vehicle implementation in reading out the preview data from a height map using an accurate GPS system in the vehicle. In this paper, a full-car model and a low-bandwidth active suspension system with passive
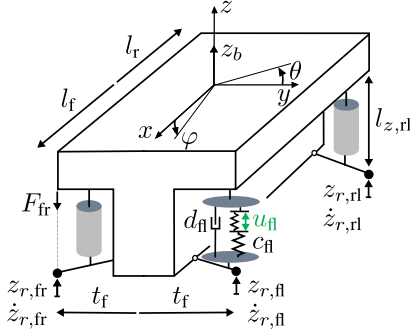
Fig. 1. Full-car model without wheel dynamics.

dampers is also considered (see Section II), and a new approach, combining a feedforward disturbance compensation calculated from the preview data with a *Skyhook* feedback controller, is proposed (see Section III). The MPC approach from [43] is also briefly summarized, since the two concepts will be compared. The further contributions of this paper are the definition of the desired preview road height profile (see Section IV), and the development of an overall concept to generate the preview road height profile, including consideration of different coordinate systems, derivation of accumulation and matching algorithms, and application of online forward–backward filtering (see Section V). Furthermore, an overall simulation environment is derived (see Section VI) and, the results of simulations (see Section VII) and vehicle implementation including a road observer (see Section VIII) are presented.

II. VEHICLE MODEL

A. Derivation of Dynamic Model

In the current literature, the common approach is to use quarter-car [10], half-car [36], or full-car models [44] with vehicle body mass and wheel mass [45]. A reduced full-car model without wheel dynamics is used for controller design in this study (see Fig. 1). This is sufficient, since actuators with a bandwidth of up to about 5 Hz are considered, which is below the eigenfrequency of the wheels of about 12 Hz and, hence, wheel dynamics cannot be influenced by the actuators. Furthermore, the vertical displacement of the wheels and the vertical velocity of the wheels are no states of the reduced model and, hence, do not have to be observed for controller implementation. This simplification does not impair controller performance, since the comfort at higher frequencies is defined by the damper characteristic and cannot be influenced by the low-bandwidth actuator.

Conservation of momentum for the vehicle body with the assumption of small angles of pitch and roll is set up, z_b is defined in an inertial coordinate system and it is assumed that the axes of pitch and roll are through the center of gravity (CE) of the vehicle body [43] (see Table I)

$$\underbrace{\begin{pmatrix} m_b & 0 & 0 \\ 0 & J_\varphi & 0 \\ 0 & 0 & J_\theta \end{pmatrix}}_{\boldsymbol{\Theta}_b} \cdot \begin{pmatrix} \ddot{z}_b \\ \ddot{\varphi} \\ \ddot{\theta} \end{pmatrix} = -\mathbf{T}_G \cdot \begin{pmatrix} F_{\mathrm{fl}} \\ F_{\mathrm{fr}} \\ F_{\mathrm{rl}} \\ F_{\mathrm{rr}} \end{pmatrix}$$

TABLE I
VARIABLES AND PARAMETERS OF THE FULL-CAR MODEL

z_b, φ, θ	heave, pitch, and roll of the vehicle body
$z_{r,ii}$	road height under the wheel ii, $ii \in \{\mathrm{fl, fr, rl, rr}\}$
$l_{z,ii}$	suspension deflection at the wheel
$\underline{z}_r$	$\left(z_{r,\mathrm{fl}} \quad z_{r,\mathrm{fr}} \quad z_{r,\mathrm{rl}} \quad z_{r,\mathrm{rr}} \right)^T$, analog for other variables
u_{ii}	actuator displacement of actuator ii
d_{ii}, c_{ii}	linearized damper, spring coefficient, $3000\, N\,s/m$, $70000\, N/m$
t_f, t_r	half of track width of front and rear axle; $0.8\, m$
l_f, l_r	wheel base from axle to CE, 1.2, $1.5\, m$
m_b	vehicle body mass, $1700\, kg$
J_φ, J_θ	pitch and roll inertia, 2500, $500\, kg \cdot m^2$
$\boldsymbol{K}_d, \boldsymbol{K}_c$	matrices comprising d_{ii}, c_{ii} in the diagonal elements

$$\mathbf{T}_G = \begin{pmatrix} 1 & 1 & 1 & 1 \\ -l_f & -l_f & l_r & l_r \\ t_f & -t_f & t_r & -t_r \end{pmatrix} \quad (2)$$

The suspension parameter $i_{d,ii}$ defines the ratio between the vertical force at the wheel and the vertical force at the damper and so accounts for the mounting position of the damper (see Fig. 1). A matrix $\boldsymbol{H}_d$, comprising the parameters $i_{d,ii}$ in the diagonal elements, and equivalently, a matrix $\boldsymbol{H}_c$ with the ratios of the spring $i_{c,ii}$ are defined. Furthermore, there are the following definitions: $\boldsymbol{T}_c = \boldsymbol{T}_G \cdot \boldsymbol{H}_c$ and $\boldsymbol{T}_d = \boldsymbol{T}_G \cdot \boldsymbol{H}_d$. Calculating spring and damper forces with the linearized coefficients c_{ii}, d_{ii} from the spring displacement and the damper velocity [43] results in the following state-space formulation for the reduced full-car model

$$\dot{\underline{x}} = \underbrace{\begin{pmatrix} \mathbf{0}_{3\times3} & \boldsymbol{I}_3 \\ -\boldsymbol{\Theta}_b^{-1}\boldsymbol{T}_c\boldsymbol{K}_c\boldsymbol{T}_c^T & -\boldsymbol{\Theta}_b^{-1}\boldsymbol{T}_d\boldsymbol{K}_d\boldsymbol{T}_d^T \end{pmatrix}}_{\boldsymbol{A}} \underline{x}$$

$$+ \underbrace{\begin{pmatrix} \mathbf{0}_{3\times4} & \mathbf{0}_{3\times4} & \mathbf{0}_{3\times4} \\ \underbrace{\boldsymbol{\Theta}_b^{-1}\boldsymbol{T}_c\boldsymbol{K}_c}_{\boldsymbol{B}_u} & \boldsymbol{\Theta}_b^{-1}\boldsymbol{T}_c\boldsymbol{K}_c\boldsymbol{H}_c & \boldsymbol{\Theta}_b^{-1}\boldsymbol{T}_d\boldsymbol{K}_d\boldsymbol{H}_d \end{pmatrix}}_{\boldsymbol{B}_w} \begin{pmatrix} \underline{u} \\ \underline{z}_r \\ \underline{\dot{z}}_r \end{pmatrix}. \quad (3)$$

This model with the states $\underline{x} = \begin{pmatrix} z_b & \varphi & \theta & \dot{z}_b & \dot{\varphi} & \dot{\theta} \end{pmatrix}^T$ is controllable, and asymptotically stable if damper coefficients are unequal to zero. The vehicle body accelerations $\ddot{z}_b, \ddot{\varphi}, \ddot{\theta}$ will be chosen as output to be minimized by the controller.

B. Experimental Validation of Vehicle Model

The derived vehicle model (3) is validated. Therefore, it is driven with the test vehicle with actuator displacement equal to zero over a road, where the height profile was accurately measured. With a highly accurate GPS-based system in the test vehicle, a mapping from the driven route to the height map is determined, and a simulation over the same height profile with the same vehicle speed can be conducted. Hence, simulated heave acceleration $\ddot{z}_b$ and pitch rate $\dot{\varphi}$ are compared to the values measured in the vehicle.

The first diagram of Fig. 2 shows the height profile of the road, while the second and third diagrams show that the calculated heave acceleration and the calculated pitch rate of the
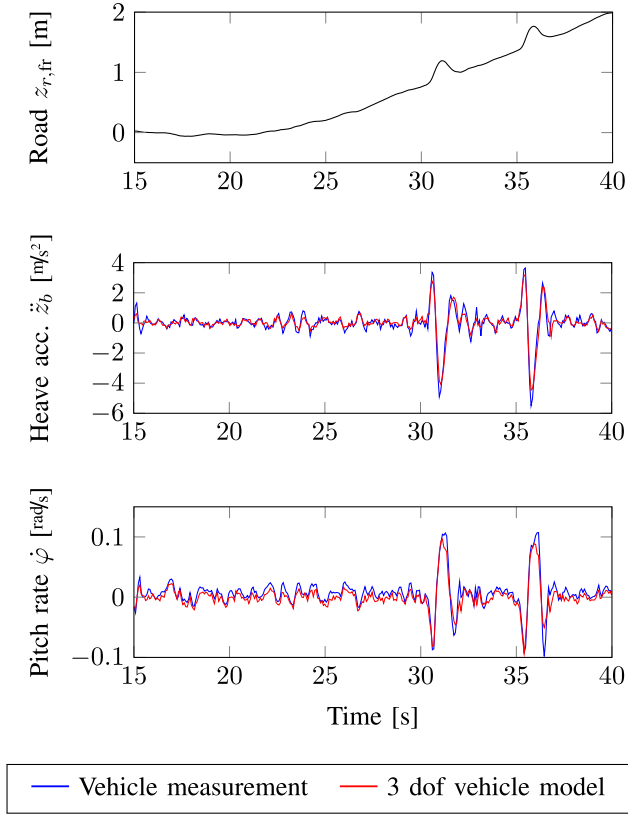
Fig. 2. Comparison of vehicle measurement and simulation driving over a road with two high road waves and a speed from 80 to 120 km/h.

simulation model correspond well with vehicle measurements in the interesting frequency range up to about 5 Hz.

III. CONTROLLER DESIGN

A. Model Predictive Control

The output $\underline{y}$, consisting of the heave $\ddot{z}_b$, pitch $\ddot{\varphi}$, and roll acceleration $\ddot{\theta}$, as well as the states $\underline{x}$ of the vehicle model (3), is predicted over a preview horizon, $\underline{\hat{y}} = \hat{\boldsymbol{\Phi}}\underline{x}[k] + \hat{\boldsymbol{\Gamma}}_{u,k}\underline{u}[k] + \hat{\boldsymbol{\Gamma}}_u\underline{\hat{u}} + \hat{\boldsymbol{\Gamma}}_w\underline{\hat{w}}$. The preview information $\underline{w} = (\underline{z}_r \;\; \underline{\dot{z}}_r)^T$ is a measured disturbance and $\hat{\bullet}$ denotes the variable over the prediction horizon, e.g., $\underline{\hat{y}} = (\underline{y}[k+1] \;\; \underline{y}[k+2] \;\; \cdots \;\; \underline{y}[k+p])^T$. The predicted output is minimized using a quadratic cost function

$$\min_{\underline{\hat{u}}} \quad \left(\underline{\hat{y}} - \underline{\hat{y}}_{\text{ref}}\right)^T \boldsymbol{Q} \left(\underline{\hat{y}} - \underline{\hat{y}}_{\text{ref}}\right) + \underline{\hat{u}}^T \boldsymbol{R}\underline{\hat{u}}. \quad (4)$$

The matrix $\boldsymbol{Q}$ weights the three accelerations by 1 and the end state by 10^5, $\boldsymbol{R}$ weights the control variables by 100. The reference values $\underline{\hat{y}}_{\text{ref}}$ for the vehicle body accelerations are zero. The reference values for the end states will be discussed in Section VII-B1. Minimizing the cost function (4) with respect to constraints on the actuator displacement and actuator displacement rate results in a quadratic program [41], [43], which is solved at each time step

$$\min_{\underline{\hat{u}}} \quad \frac{1}{2}\underline{\hat{u}}^T \left(\hat{\boldsymbol{\Gamma}}_u^T \boldsymbol{Q}\hat{\boldsymbol{\Gamma}}_u + \boldsymbol{R}\right) \underline{\hat{u}} + \left(\underline{x}[k]^T \hat{\boldsymbol{\Phi}}^T \boldsymbol{Q}\hat{\boldsymbol{\Gamma}}_u \right.$$
$$\left. + \underline{u}[k]^T \hat{\boldsymbol{\Gamma}}_{u,k}^T \boldsymbol{Q}\hat{\boldsymbol{\Gamma}}_u + \underline{\hat{w}}^T \hat{\boldsymbol{\Gamma}}_w^T \boldsymbol{Q}\hat{\boldsymbol{\Gamma}}_u - \underline{\hat{y}}_{\text{ref}}^T \boldsymbol{Q}\hat{\boldsymbol{\Gamma}}_u\right) \underline{\hat{u}}$$

s.t. $\quad \underline{\hat{u}}_{\min} \le \underline{\hat{u}} \le \underline{\hat{u}}_{\max}$

$$\Delta\underline{\hat{u}}_{\min} \le \Delta\underline{\hat{u}} \le \Delta\underline{\hat{u}}_{\max}. \quad (5)$$

Carrying out this optimization, optimal control variables for each time step over the preview horizon are calculated, and the control variables for the four actuators for the next time step are applied. The optimization is calculated again at the next time step with adapted initial states and a shifted road height profile.

B. Feedforward Disturbance Compensation

In this section, a second control approach is proposed, compensating for the road height profile $\underline{z}_r$, $\underline{\dot{z}}_r$, which is the known disturbance measured by the preview sensor, with the actuator motion $\underline{u}_0$ in (3). The result of the last three equations is

$$\boldsymbol{T}_c\boldsymbol{K}_c\underline{u}_0 + \boldsymbol{T}_c\boldsymbol{K}_c\boldsymbol{H}_c\underline{z}_r + \boldsymbol{T}_d\boldsymbol{K}_d\boldsymbol{H}_d\underline{\dot{z}}_r = \underline{0}. \quad (6)$$

Since there are four actuators for three vehicle body motions, an additional degree of freedom can be chosen. This compensation can also be interpreted as an inverse vehicle model with the input of the road height profile $\underline{z}_r$, $\underline{\dot{z}}_r$, and the requirement of vehicle body motion z_b, φ, θ equal to zero. The calculated outputs are the corresponding actuator displacements $\underline{u}_0$.

Eliminating warp in the vehicle body is proposed to define the additional degree of freedom [43], which means that, on a flat road, with vehicle body states being equal to zero, all actuators apply the same force. Therefore, the sum of the front left and rear right actuators is defined as being equal to the sum of the forces of the front right and rear left actuators for the vehicle body states equal to zero

$$\begin{pmatrix} -1 & 1 & 1 & -1 \end{pmatrix} \boldsymbol{K}_c \left(-\boldsymbol{H}_c\underline{z}_r - \underline{u}_0\right) = 0. \quad (7)$$

Combining (6) and (7), the actuator displacements are calculated as follows:

$$\underline{u}_0 = -\begin{pmatrix} \boldsymbol{T}_c\boldsymbol{K}_c \\ \begin{pmatrix} -1 & 1 & 1 & -1 \end{pmatrix}\boldsymbol{K}_c \end{pmatrix}^{-1} \cdot$$
$$\left(\begin{pmatrix} \boldsymbol{T}_c\boldsymbol{K}_c\boldsymbol{H}_c \\ \begin{pmatrix} -1 & 1 & 1 & -1 \end{pmatrix}\boldsymbol{K}_c\boldsymbol{H}_c \end{pmatrix}\underline{z}_r + \begin{pmatrix} \boldsymbol{T}_d\boldsymbol{K}_d\boldsymbol{H}_d \\ \underline{0}_{1\times4} \end{pmatrix}\underline{\dot{z}}_r\right). \quad (8)$$

This is a feedforward control calculated from the road height profile and its first derivative to eliminate vehicle body motions. In contrast to the MPC, which has the road height profile over a preview horizon as input, only the road height values under the wheels are used. The feedforward compensation cannot incorporate actuator constraints, and so the road height profile is shaped accordingly in order to only contain frequencies which should, and which can be, compensated for by the actuators.

This feedforward control is added to the actuator signal from a *Skyhook* controller. This complements well, since for a good preview signal, the feedforward part reduces vehicle body motions, so the *Skyhook* control loop generates a reduced actuator signal.

IV. DEFINITION OF DESIRED ROAD HEIGHT PROFILE

In this section, a desired road height profile for the feedforward control is defined, which only contains frequencies which
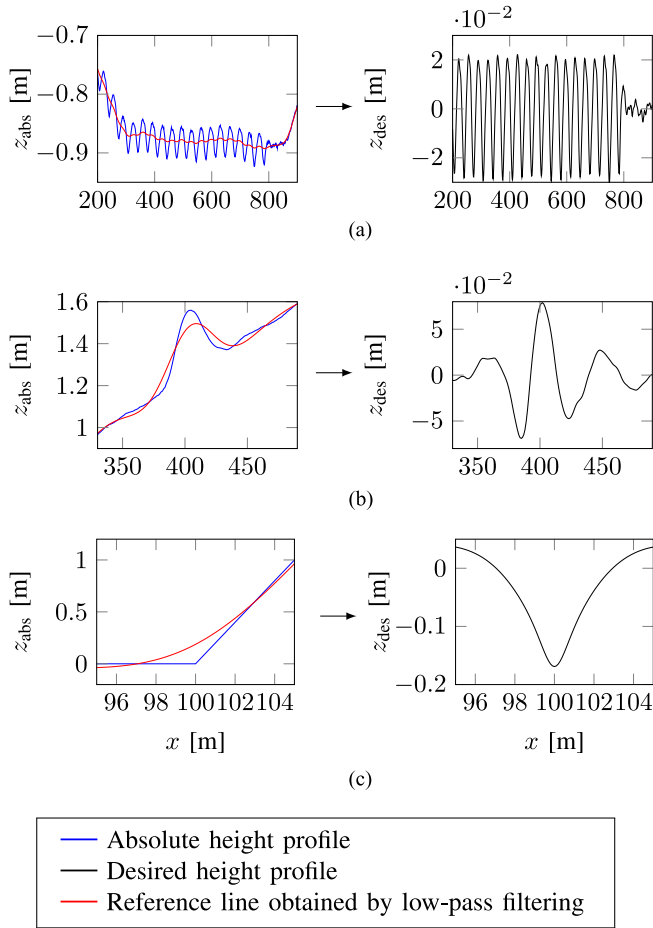
Fig. 3.   Definition of desired road height profile calculated from the absolute road height profile by high-pass and low-pass filtering. (a) Road waves with period of 35 m at 120 km/h. (b) High road wave with 45 m length at 100 km/h. (c) Rising road at 30 km/h.

should be compensated for by the actuators. A band-pass filter is chosen to obtain the desired road profile, since low frequencies are hardly perceptible by the driver, and high frequencies are not feasible for the actuators.

The road height profile over normal height zero is called an absolute road height profile, where the offset to zero is not important and, hence, ignored. To obtain the desired road height profile z_{des}, the absolute road height profile as a function of the traveled distance $z_{abs}(x)$ is converted to a function of time $z_{abs}(t)$, where the vehicle speed is known, and a high-pass and low-pass forward–backward filtering is conducted. Forward–backward filtering allows for filtering without phase distortion, but the signal needs to be available for the future. This forward–backward filtering for exemplary roads is presented in Fig. 3, where the entire road profile is used as input for the filter. High-pass filtering without phase distortion equals to low-pass filtering with the same frequency and calculation of the difference of the filtered and the original signal. Hence, there is a reference line, obtained by low-pass filtering the profile depicted in Fig. 3 for better understanding.

Road waves with a period of 35 m and a peak-to-peak amplitude of 4 cm are depicted in Fig. 3(a), as well as the resulting desired height profile. When driving at high speed, the low-bandwidth actuators under consideration can only compensate
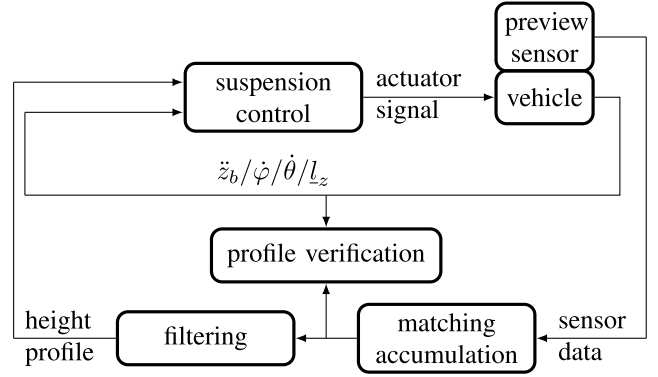

Fig. 4.   Overview of overall concept.

for long road waves, which correspond to an excitation below about 5 Hz. Driving more slowly over the same road waves in Fig. 3(a) would result in a desired road height profile with a lesser amplitude, which makes sense, since these road waves are less apparent to the driver at slower speeds.

A high road wave, 30 cm in height and 45 m in length, is depicted in Fig. 3(b). In the resulting desired road height profile, the road elevation is represented first by a negative and, then, by a positive elevation, which used as an input for the derived feedforward compensation (8), provokes a lifting of the vehicle in front of the road elevation to increase actuator travel.

Fig. 3(c) shows that a rising road profile is eliminated by applying the high-pass filter, and the resulting desired profile can be used as input for the feedforward control (8) without exceeding actuator constraints.

How to obtain the road profile desired if the absolute road profile is given for the entire road was defined in this section. The following section describes new methods to generate the same desired road profile using measurements of a moving vehicle body fixed sensor with limited preview.

V. Generation of Road Height Profile With Vehicle Sensors

As presented in the introduction, the main focus in the current literature consists of controller design for preview active suspension systems. In this study, an overall concept, consisting of road profile generation from the sensor data, profile verification using vehicle measurements, and suspension control, is proposed (see Fig. 4). A camera mounted behind the windshield is used, so that road segments are measured redundantly at different time steps, since the sensor in this example measures the road between 4 m and 18 m in front of the front axle (fa) and determines a new measurement every 50 ms.

A. Coordinate Systems to Generate the Road Height Profile

Since the sensor moves with the vehicle body, the measurement of the road for two consecutive time steps will not be in alignment, but the redundant measurements can be used to accumulate the height values in order to reduce sensor noise. The first proposal is to transform the height map of the previous time step so that it aligns with the measurements of the current time
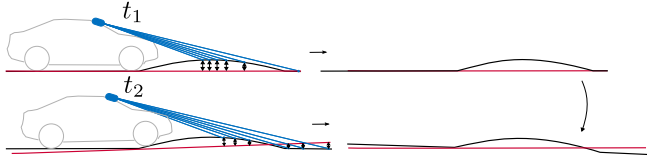
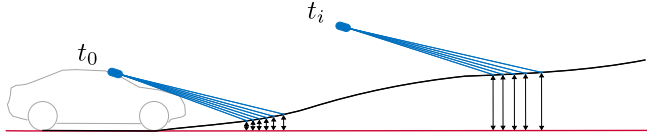Fig. 5. Sensor-fixed compilation of sensor measurements, road profile in black, reference plane in red.

Fig. 6. Inertial-fixed accumulation of sensor measurements, road profile in black, reference plane in red.

Fig. 7. Accumulation of sensor measurements in a discrete shift register.

step and the overlapping road segments are accumulated. This approach is depicted in Fig. 5 and detailed as follows.

1) The distances from the sensor to the road measured at time step t_1 are converted to road heights relative to a sensor-fixed reference plane.
2) In the next time step t_2, the measured distances from the sensor are again used to obtain height values relative to the sensor-fixed reference plane. Due to vehicle body motion, the orientation of the sensor-fixed reference plane compared to the road is changed.
3) A transformation of the height map from time step t_1 to align with the new heights of time step t_2 is conducted.
4) The heights measured at two time steps from a different point of view are accumulated to enhance accuracy.

The sensor-fixed reference plane is defined to align with the even road for the vehicle in a steady state. Other sensor-fixed orientations are also possible.

Second, an inertial coordinate system is proposed to compile the sensor measurements (see Fig. 6). Therefore, an inertial-fixed reference plane is defined at the beginning, and the distances measured from the sensor to the road are converted to heights relative to the inertial-fixed plane. Thus, the new measurements are transformed to align with the existing height map. The inertial-fixed reference plane can be adapted if the height values exceed the limits of the data type, and this change of the offset is also conducted for the states of the MPC.

Both concepts for compiling the sensor measurements result in a height profile, which contains all the information of the road for the given preview horizon. The height profile of the first approach changes its orientation in the coordinate system at each time step, the height profile of the second approach is consistent in the coordinate system for consecutive time steps.

B. Accumulation of Height Values

A discretized height map with values h_1 to h_k from the past to the preview distance is generated in a shift register (see Fig. 7). The values of the past are needed for the filtering to be discussed later. The shift register is shifted by the traveled distance between two time steps calculated from the vehicle speed v, height values in the past are removed and new ones are added.
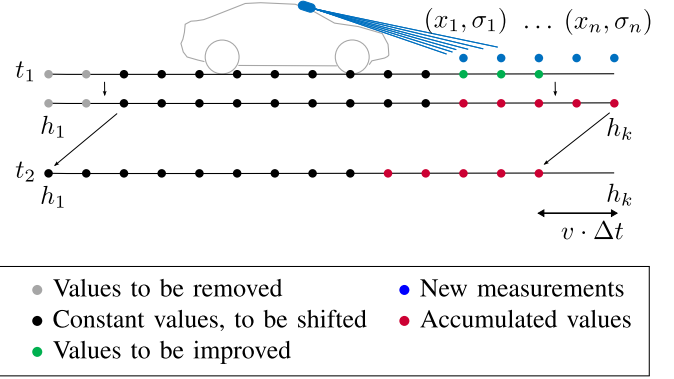
It is assumed that the different sensor measurements at one time step have different known standard deviations which increase with the distance. Using the maximum-likelihood estimation [46], [47] is proposed to calculate the mean μ for the height of one cell from different measurements x_i with a particular known standard deviation σ_i.

The probability density function of a normal distribution with mean μ and standard deviation σ_i reads

$$f_i\left(x_i \mid \mu, \sigma_i^2\right) = \frac{1}{\sqrt{2\pi\sigma_i^2}} \exp\left(-\frac{(x_i - \mu)^2}{2\sigma_i^2}\right). \quad (9)$$

The likelihood-function $L(\mu)$ is calculated from the product of the probability density functions (9) of all n measurements

$$L(\mu) = \prod_{i=1}^{n} \frac{1}{\sqrt{2\pi\sigma_i^2}} \exp\left(-\sum_{i=1}^{n} \frac{(x_i - \mu)^2}{2\sigma_i^2}\right). \quad (10)$$

The maximum of the function $L(\mu)$ indicates the most probable mean for the given measurements. To determine the maximum of the function, a derivative with respect to μ is calculated, and the resulting expression is set to zero. This is easier to deduce using the logarithm of $L(\mu)$ and the result remains the same, since the logarithm is a monotonically increasing function

$$\frac{\partial}{\partial\mu}\log L(\mu) = \sum_{i=1}^{n} \frac{x_i - \mu}{\sigma_i^2} \overset{!}{=} 0. \quad (11)$$

Solving for μ results in

$$\mu = \frac{\sum_{i=1}^{n} \frac{x_i}{\sigma_i^2}}{\sum_{i=1}^{n} \frac{1}{\sigma_i^2}}. \quad (12)$$

If the standard deviations σ_i are identical, the arithmetic mean results from (12). A Kalman filter [48] with a constant prediction model for the height in the cell, zero process noise, and the measurement noise equal to the square of the known measurement standard deviation results in the same as (12), if the initial state is set to the first measurement, and the initial covariance matrix to set to the square of the standard deviation.

C. Transformation of Sensor Measurements

The actual sensor measurements, converted to height values relative to a sensor-fixed reference plane, as described in Section V-A, are shifted and rotated compared to the height

- Height map at time k for equidistant points
- Sensor measurements at time $k+1$ converted to height values relative to a sensor-fixed reference plane
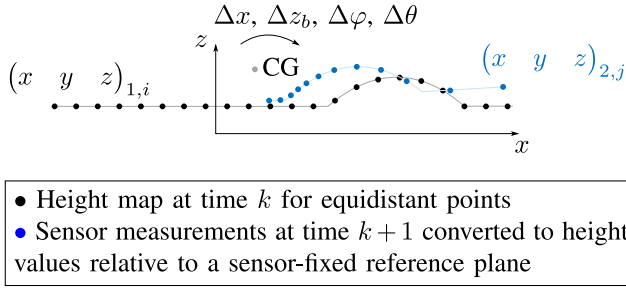
Fig. 8.   Transformation of sensor measurements based on matching.

map of the previous sampling instance (see Fig. 8). To align the black curve with the blue curve for accumulation of height values, the black curve can be rotated about any point, which results in different shifting values. In the following section, the profile is rotated about the CG of the vehicle body. This allows the information to be combined with other measurements.

If the vehicle body motions Δx, Δz_b, $\Delta \varphi$, $\Delta \theta$ are exactly known, the transformation of the height values can be calculated. Since a high degree of accuracy is needed, the transformation is calculated, using an initial guess, by matching the sensor data of two time steps. Aligning the curves in Fig. 8 without an initial guess is hard to compute, since the data association of the new measurements with the values of the height map is not known. Calculating the driven distance Δx from the measured vehicle speed simplifies the matching, since the data association is fixed. A least mean square fit [49] of the associated points assuming small angles is sought

$$
\min_{\Delta z_b, \Delta \varphi, \Delta \theta} \quad \sum_{k=1}^{K} \left(\Delta \varphi \left(x_{1,k} - x_{\mathrm{CG}} - \Delta x \right) \right.
$$
$$
\left. - \Delta \theta \left(y_{1,k} - y_{\mathrm{CG}} \right) - \Delta z_b + z_{1,k} - z_{2,k} \right)^2 . \quad (13)
$$

Derivation with respect to the optimization variables $\underline{x} = \left(\Delta z_b \quad \Delta \varphi \quad \Delta \theta \right)^T$, and setting the result to zero results in the following system of linear equations:

$$
\boldsymbol{E}^T \boldsymbol{E} \underline{x} = -\boldsymbol{E}^T \underline{e}
$$
$$
\boldsymbol{E} = \begin{pmatrix} -1 & (x_{1,1} - x_{\mathrm{CG}} - \Delta x) & -(y_{1,1} - y_{\mathrm{CG}}) \\ \vdots & \vdots & \vdots \\ -1 & (x_{1,K} - x_{\mathrm{CG}} - \Delta x) & -(y_{1,K} - y_{\mathrm{CG}}) \end{pmatrix}
$$
$$
\underline{e} = \begin{pmatrix} z_{1,1} - z_{2,1} \\ \vdots \\ z_{1,K} - z_{2,K} \end{pmatrix} . \quad (14)
$$

With the calculated values Δz_b, $\Delta \varphi$, $\Delta \theta$, the transformation of the height map of the previous instance can be conducted. To incorporate the accuracy of every height value, the K summands in (13) are weighted with $1/(\mathrm{Var}(z_{1,k}) + \mathrm{Var}(z_{2,k}))$.

D. Filtering of the Height Profile

w For the sensor-fixed compilation (see Section V-A), the height profile is orientated differently in the coordinate system at each time step due to vehicle body motion. The idea proposed in this paper is to eliminate this by a forward–backward high-pass filtering of the road profile from the past to the preview distance at each time step. Hence, the requirement of Section IV, that only frequencies over a defined threshold should remain in the desired height profile, is also achieved. Furthermore, a low-pass forward–backward filtering is conducted to smooth the profile. The forward–backward filtering is detailed in this section. The difference equation of a linear discrete filter with order k reads [50]

$$
y[n] = b_0 \cdot x[n] + b_1 \cdot x[n-1] + \ldots + b_k \cdot x[n-k]
$$
$$
- a_1 \cdot y[n-1] - \ldots - a_k \cdot y[n-k]. \quad (15)
$$

The filter is realized in direct form II for minimal number of used delays

$$
y[n] = b_0 \cdot x[n] + z_1[n-1]
$$
$$
z_1[n] = b_1 \cdot x[n] + z_2[n-1] - a_1 \cdot y[n]
$$
$$
\vdots
$$
$$
z_{k-1}[n] = b_{k-1} \cdot x[n] + z_k[n-1] - a_{k-1} \cdot y[n]
$$
$$
z_k[n] = b_k \cdot x[n] - a_k \cdot y[n]. \quad (16)
$$

Using forward–backward filtering, the question arises of how to determine the initial states of the filter for both the forward and the backward filtering step. By definition, the initial states are the steady states of the filter for the first input to minimize transient oscillation of the filter [51]. Setting the constant states $z_1[n] = z_1[n-1] \cdots z_k[n] = z_k[n-1]$ into (16) results in the following system of linear equations, which is solved once for the chosen filter:

$$
\begin{pmatrix} 1+a_1 & -1 & & & \\ a_2 & 1 & -1 & & \\ \vdots & & \ddots & & \\ a_{k-1} & & & 1 & -1 \\ a_k & & & & 1 \end{pmatrix} \begin{pmatrix} \frac{z_1[n]}{x[n]} \\ \frac{z_2[n]}{x[n]} \\ \vdots \\ \frac{z_{k-1}[n]}{x[n]} \\ \frac{z_k[n]}{x[n]} \end{pmatrix} = \begin{pmatrix} b_1 - a_1 b_0 \\ b_2 - a_2 b_0 \\ \vdots \\ b_{k-1} - a_{k-1} b_0 \\ b_k - a_k b_0 \end{pmatrix} .
$$
$$
(17)
$$

VI. DESIGN OF SIMULATION ENVIRONMENT

A simulation environment is set up with a vertical model of the vehicle driving over a defined road to test the proposed algorithms. With the simulated heave, pitch, and roll of the vehicle body, the position of the sensor can be calculated and, hence, the measured distances from the sensor to the road. This
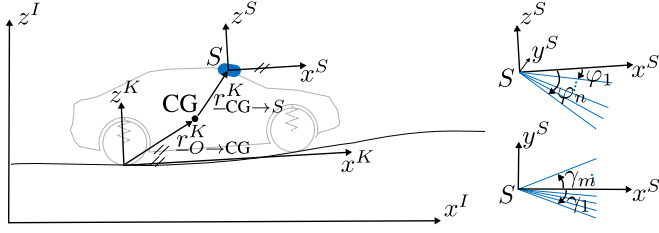
Fig. 9. Definition of vectors and coordinate systems.

Fig. 10. Calculation of exact sensor measurements, driving over road waves with period of 35 m at 120 km/h.

is used to simulate the generation of the height profile and the suspension control in the closed loop.

The road is given in an inertial coordinate system I. In addition, a vehicle body fixed coordinate system K with the origin on the road and in the middle of the rear axle, as well as a vehicle body fixed coordinate system with the origin in the sensor S, is defined (see Fig. 9). It is assumed that the vehicle body pitches and rolls about the CG. A principal sensor model is used, where sensor measurements are defined by the angles $\varphi_1, \ldots, \varphi_n$ with respect to the y^S-axes and $\gamma_1, \ldots, \gamma_m$ with respect to the z^S-axes. The distance measured along the axis defined by the angles can represent the time-of-flight measurement of a laser sensor or the distance information from disparity calculation of a camera.

The heave position z_b is simulated with respect to the inertial coordinate system I, and is zero at the beginning of the simulation. To obtain the vertical position of the CE, the height of the CE needs to be added. The value x_{ra} denotes the x-position of the rear axle, obtained by the integration of the defined vehicle speed. The position of the sensor in the inertial coordinate system I is calculated

$$
\underline{r}_{O \to S}^I = \begin{pmatrix} x_{\mathrm{ra}} \\ 0 \\ z_b \end{pmatrix} + \underline{r}_{O \to \mathrm{CG}}^K
$$
$$
+ \underbrace{\begin{pmatrix} 1 & 0 & 0 \\ 0 & \cos\theta & -\sin\theta \\ 0 & \sin\theta & \cos\theta \end{pmatrix} \begin{pmatrix} \cos\varphi & 0 & \sin\varphi \\ 0 & 1 & 0 \\ -\sin\varphi & 0 & \cos\varphi \end{pmatrix}}_{\boldsymbol{R}_{\theta\varphi}} \underline{r}_{\mathrm{CG} \to S}^K .
$$

(18)

The equation of the axis of one distance measurement is defined by the sensor (18), and a direction vector $\underline{n}_{ij}^I = \boldsymbol{R}_{\theta\varphi} \cdot \underline{n}_{ij}^K$ for every axis with the angles φ_i $(i \in \{1, \cdots, n\})$ and γ_j $(j \in \{1, \cdots, m\})$

$$
\underline{n}_{ij}^K = \begin{pmatrix} \cos\varphi_i & 0 & \sin\varphi_i \\ 0 & 1 & 0 \\ -\sin\varphi_i & 0 & \cos\varphi_i \end{pmatrix} \begin{pmatrix} \cos\gamma_j & -\sin\gamma_j & 0 \\ \sin\gamma_j & \cos\gamma_j & 0 \\ 0 & 0 & 1 \end{pmatrix}
$$
$$
\times \begin{pmatrix} 1 \\ 0 \\ 0 \end{pmatrix} .
$$

(19)

With the equation of the axis of the distance measurement in the inertial coordinate system, the point of intersection with the road surface, given as matrix $(x, y, z)^I$, is sought iteratively using nested intervals. Hence, an exact distance d_{ij} between the
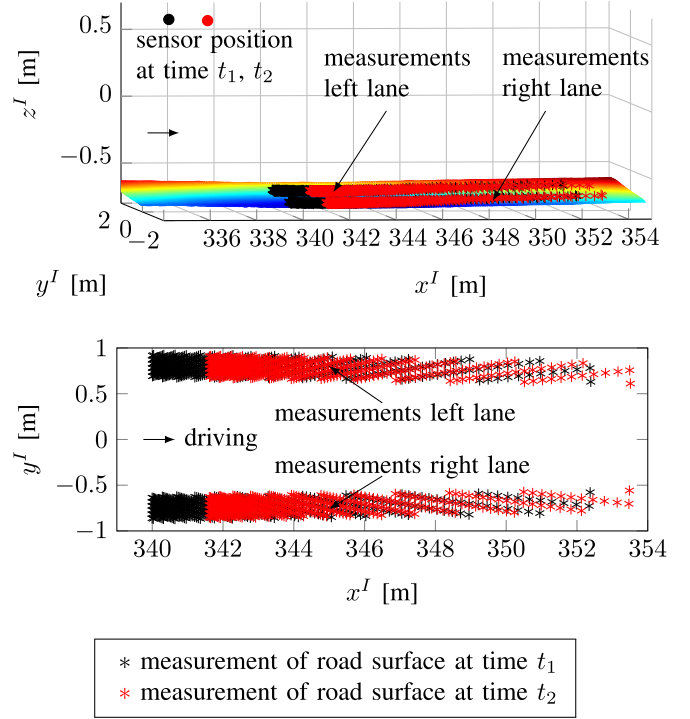
sensor position and the road surface is calculated, and the noise is added to represent the specifications of a real sensor.

Different sensors at different positions of the vehicle can be simulated. In this study, a camera behind the windshield (see Fig. 7) is simulated exemplarily, measuring about 800 distances every 50 ms in the area in front of the wheels for a width of 25 cm from 4 m to 18 m in front of the front axle. These specifications are feasible for an automotive camera with about 1000×1000 pixels, if the software and the computing hardware is adapted to evaluate that amount of disparities of the road surface.

The simulation of exact sensor measurements of the defined sensor is demonstrated in Fig. 10. The first diagram shows the sensor position at two time steps, and the calculated exact measurements on the given road. The second diagram shows the sensor measurements in a top view.

VII. SIMULATION RESULTS

A nonlinear simulation model is used to show the effects of the derived controllers.

A. Comparison of MPC and Feedforward Compensation in Terms of Actuator Constraints

First, the MPC approach with the incorporated actuator constraints (5) is compared to the feedforward control approach (8) for driving over the high road obstacle from Fig. 3(b) at 100 km/h. The first diagram of Fig. 11 shows the road profile, which is assumed to be known exactly as input for the preview controllers. Since the road elevation is too high for the limited actuator displacement, the MPC approach lifts the vehicle as soon as the obstacle comes in sight in order to increase actuator
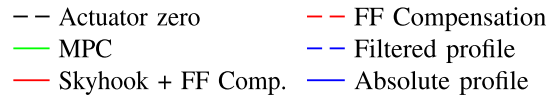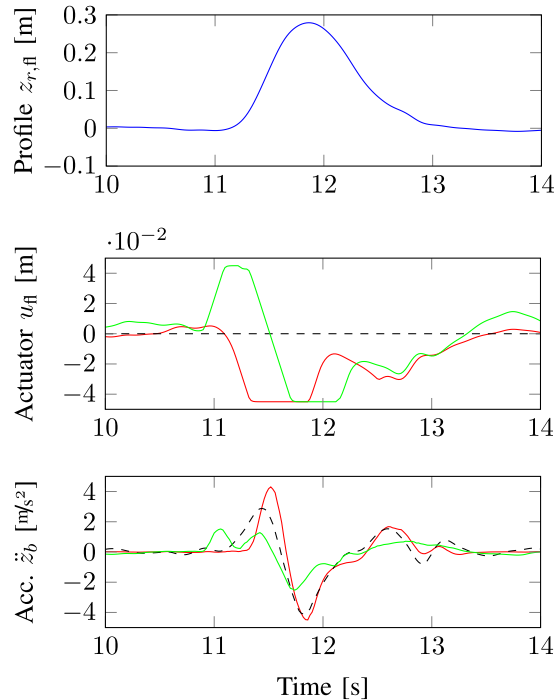
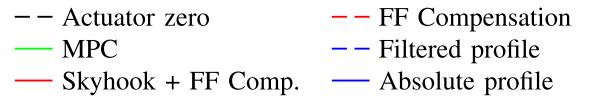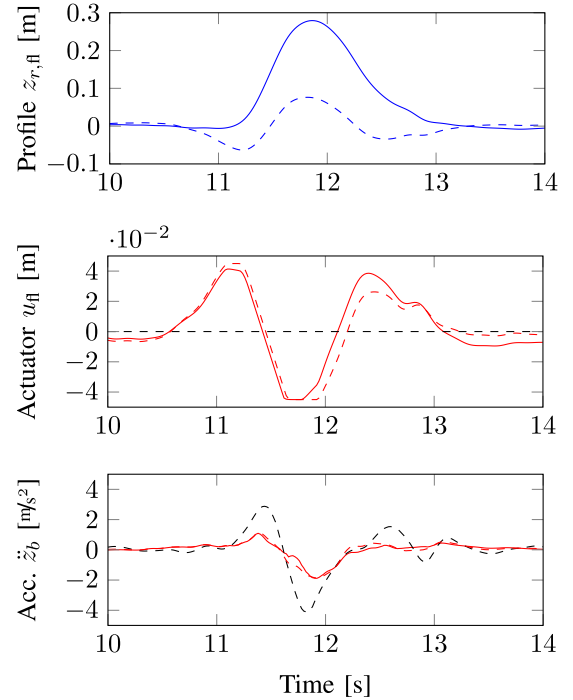Fig. 11.   Absolute profile as controller input.

Fig. 12.   Filtered profile as controller input.

travel. Preview for the MPC was chosen as 0.5 s. The actuator displacement of the feedforward compensation is saturated, while driving over this road elevation, and even in combination with the *Skyhook* feedback control, which reduces the negative effects of the feedforward part, the performance is worse than without actuator motion for this road signal as input.

In Fig. 12, the same simulation is performed, but the height profile is filtered, as proposed in Section IV, so that the performance of the feedforward compensation is equal to the MPC. Hence, for this obstacle, the feedforward compensation with the desired road height profile as input will result in the same performance as the MPC for both, the absolute and the desired road height profile. The necessary preview length for the filtering on the one hand, and the MPC approach on the other hand, will be discussed in the next Section.

B. Comparison of MPC and Feedforward Compensation in Terms of Preview Length

1) Inertial Height Profile and MPC: Two concepts of combining the derived controllers with the presented approaches to generate the road height profile were proposed. The first concept consists of an inertial-fixed compiled height profile (see Fig. 6), which is the input to the MPC (see Section III-A). This works, since the MPC is set up to minimize vehicle body accelerations incorporating constraints on actuator displacement and actuator displacement rate. To ensure return to equilibrium, the end states are additionally weighted in (4). In this approach,

they cannot be weighted to zero, since the heave position in the inertial coordinate system is a state of the system and needs to have an offset to zero, as does the height profile in the first diagram of Fig. 13. Instead, a straight line is fitted in the height profile from the past to the preview distance using least squares, and the heave position at the end of the prediction horizon is weighted to the height value of the straight line at this position.

Simulation results for driving over the sinus-shaped road waves with a period of 35 m and a peak-to-peak amplitude of 4 cm at 120 km/h are shown in Fig. 13. The preview is chosen 0.25 s in front of every wheel, which corresponds to 8.3 m at that speed. The inertial road profile, which is the input to the MPC and the nonlinear simulation model, is depicted in the first diagram, as well as the preview distance in front of the fa, which is far less than the length of the road wave. The second diagram shows the actuator displacement, which is, despite the drift in the inertial height profile, around zero and within the actuator bounds. The reduction of the heave acceleration, obtained by the preview MPC compared to a controller without preview, is shown in the third diagram, which is at a peak of -65%.

2) Sensor-Fixed Height Profile and Feedforward Control: A second concept is proposed, which consists of the following steps.

1) Compilation of the sensor measurements in a sensor-fixed coordinate system (see Fig. 5).
2) Matching of the measurments to determine the transformation between two time steps using (14).
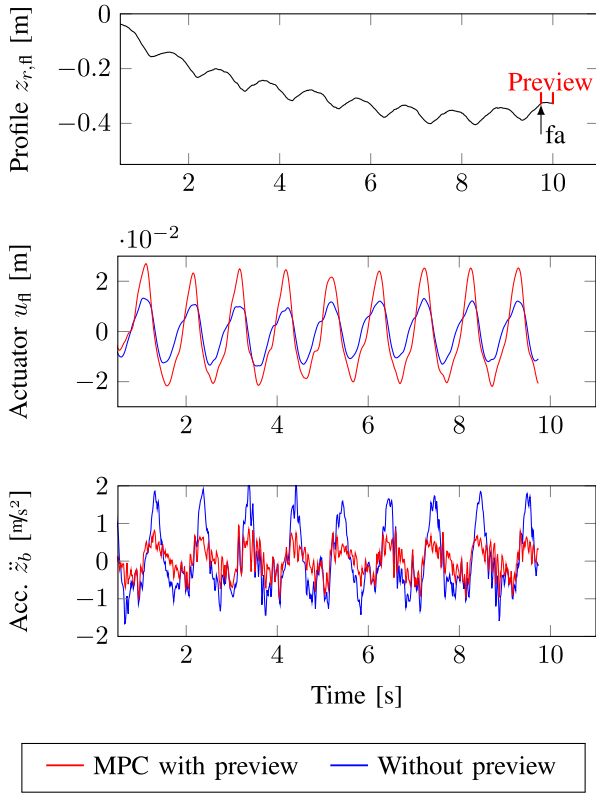
Fig. 13. Simulation of MPC with exact inertial-fixed height profile as input and 0.25 s preview, driving over road waves with period of 35 m at 120 km/h.
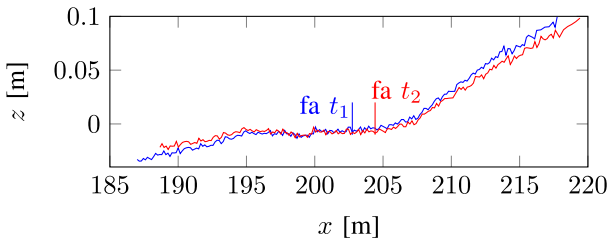

Fig. 14. Sensor-fixed compilation, height profile in the vehicle body fixed coordinate system K at two time steps.

3) Forward–backward high-pass and low-pass filtering (see Section V-D) of the height profile from the past to the preview distance.
4) Low-pass filtering of the height values over time. The height values at a certain distance in front of the wheels are filtered to compensate for the phase delay and to obtain the filtered height values under the wheels.
5) Calculating a feedforward control from the height values under the wheels using (8).
6) Adding the feedforward preview control to the signal of a feedback *Skyhook* controller without preview (1).

Simulation results are shown in the following section using the simulation environment presented in Section VI, with the described exemplary sensor. For each sensor measurement, a noise with normal distribution and standard deviation of 5 cm is added. This results in an error of up to 20 cm. A height map is compiled from -15 to 15 m with respect to the fa with a cell length of 15 cm. The compiled height profile for driving over the road waves from Fig. 13 is shown for two time steps in Fig. 14
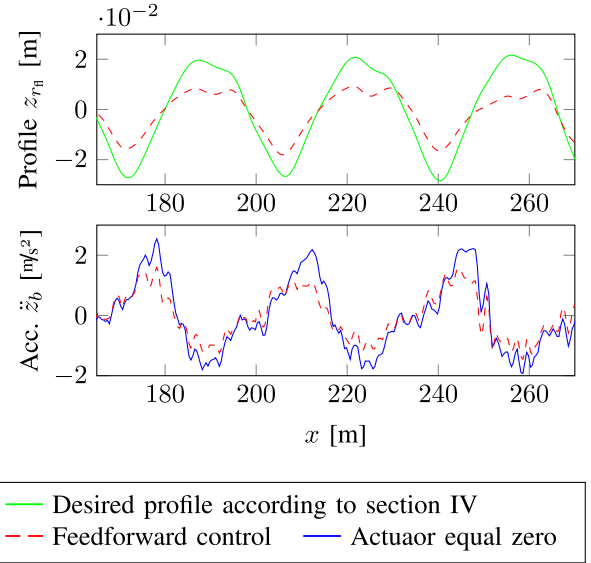

Fig. 15. Simulation of generation of the height profile from camera measurements with an added noise and suspension control, driving over road waves with a 35 m period at 120 km/h.

with the corresponding position of the fa. Since the profile is sensor fixed, it is rotated differently in the coordinate system for the two time steps. The road wave is not entirely captured within the preview range.

The first diagram in Fig. 15 shows the desired road profile from Fig. 3(a) in green and the obtained road profile using the simulated measurements with the added noise after matching, accumulation, and filtering. It can be observed that the high-pass filter eliminates the different orientation of the profile for the different time steps. The amplitude is smaller than desired because of the limited preview.

The second diagram shows that the feedforward control reduces the heave acceleration compared to actuator displacement equal to zero. An addition of a *Skyhook* controller will further improve the performance. Since a preview of 15 m was available for the filtering and the preview for the MPC in Fig. 13 was about 8 m with a slightly better result, it is shown that less preview provides the same results for the MPC approach. If the preview range for the filtering is decreased, the amplitude of the resulting road waves in Fig. 15 will decrease further, thus reducing performance. A higher cut-off frequency for high-pass filtering results in a lower necessary preview range, but also limits the effects of the preview control, since only higher frequent road disturbances are represented in the profile.

It was also shown in Fig. 15 that the feedforward control is robust because of the accumulation of sensor measurements with normal distributed noise. However, it is necessary to get a smooth profile after accumulation, either with few accurate or more less-accurate measurements.

Two overall concepts, using a MPC and an inertial-fixed height profile, as well as a feedforward control and a sensor-fixed height profile, were presented. Both concepts produce the same performance (see Figs. 11 and 12) and less preview is required for the MPC (see Fig. 13), but the second approach is better suited to modularize the controller. An active suspension controller also needs to reduce the pitch and roll motion, while

turning and accelerating. Using the feedforward disturbance compensation, independent modules can be used and the signals can be added, since the feedforward control only compensates for the road unevenness. In contrast, while turning on a flat road, the arising roll angle will be further increased by the MPC (4), in order to minimize roll acceleration, instead of reducing the roll angle, which is desired for good handling characteristics. Hence, all the functionality of the active suspension system at turning, accelerating, and for good ride comfort needs to be incorporated in the optimization by adapting the reference trajectories for the vehicle states over the preview horizon in (4) in order to obtain desired roll and pitch motion, while turning and accelerating. This is much harder to adjust for all possible driving situations, which can occur in comparison to a controller with a roll module, a pitch module, a *Skyhook* module, and a preview module, which can all be set up independently from each other.

VIII. Vehicle Implementation

In this section, the results of implementing the second proposed concept with sensor-fixed accumulation and a feedforward control in a vehicle using a camera to detect the road profile will be presented. In addition, an observer to verify the camera measurements with the vehicle body motion will be proposed.

A. Measurement Results

In Fig. 16, measurements for driving over the pictured road wave at 20 km/h with a test vehicle with a low-bandwidth active suspension and a camera is presented. It shows that a *Skyhook* controller without preview noticeably reduces the pitch rate and slightly reduces the heave acceleration of the vehicle body. A reduction of up to -80% compared to the system without actuator motion is feasible by applying the feedforward control.

These reductions of vehicle body motions are clearly sensible for the driver, since the road obstacle is barely noticeable, while driving with the preview control.

B. Observer of Road Height Profile

In this section, an observer is proposed to determine the road height profile under the wheels from the vehicle motion and independently from the preview sensor. This signal cannot be used for preview control of the front axle, since it is available with a time delay, but it can be used to verify the preview signal, either online, to deactivate the preview functionality if implausible signals occur, or offline, to generate a reference height profile to optimize the algorithms.

A disturbance observer is proposed using the vehicle model (3)

$$\dot{\underline{x}} = \boldsymbol{A}\underline{x} + \boldsymbol{B}_u \underline{u} + \boldsymbol{B}_w \begin{pmatrix} \underline{z}_r \\ \dot{\underline{z}}_r \end{pmatrix}, \qquad \underline{x}(0) = \underline{x}_0 \qquad (20)$$

With the road excitation $\underline{w} = (\underline{z}_r \quad \dot{\underline{z}}_r)^T$ and its dynamic

$$\dot{\underline{w}} = \underbrace{\begin{pmatrix} \boldsymbol{0}_4 & \boldsymbol{I}_4 \\ \boldsymbol{0}_4 & \boldsymbol{0}_4 \end{pmatrix}}_{\boldsymbol{W}} \underline{w}, \qquad \underline{w}(0) = \underline{w}_0 \qquad (21)$$
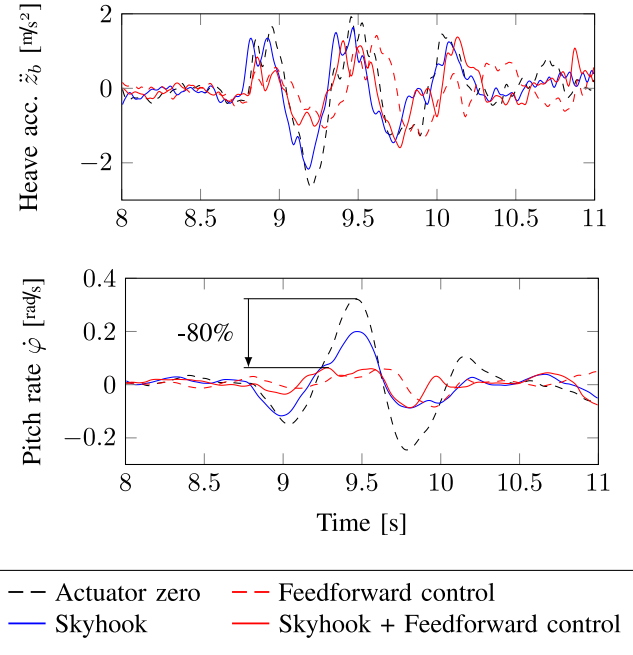

Fig. 16.   Reduction of heave acceleration and pitch rate driving over a road wave at 20 km/h.
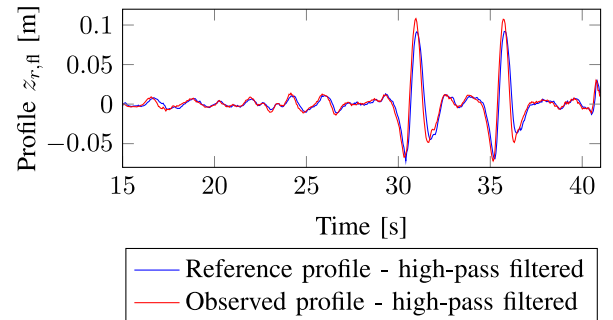

Fig. 17.   Observed height profile driving over the road with two high road elevations at 70 to 120 km/h.

the state space is augmented

$$\begin{pmatrix} \dot{\underline{x}} \\ \dot{\underline{w}} \end{pmatrix} = \begin{pmatrix} \boldsymbol{A} & \boldsymbol{B}_w \\ \boldsymbol{0}_{8 \times 6} & \boldsymbol{W} \end{pmatrix} \begin{pmatrix} \underline{x} \\ \underline{w} \end{pmatrix} + \begin{pmatrix} \boldsymbol{B}_u \\ \boldsymbol{0}_{8 \times 4} \end{pmatrix} \underline{u}. \qquad (22)$$

The available measurement signals in the vehicle are the pitch rate $\dot{\varphi}$, the roll rate $\dot{\theta}$, the heave acceleration $\ddot{z}_b$, the four suspension deflections $l_{z,ii}$, and the actuator displacement $\underline{u}$. These signals are used to correct the prediction of the model (22) using a Kalman filter [48]. Since the suspension deflection often suffers from an offset, its first derivative is used to correct the model. The corresponding output of the model (22), which is

corrected by the measurements, is calculated as follows:

$$
\begin{pmatrix} \dot{\varphi} \\ \dot{\theta} \\ \ddot{z}_b \\ \dot{\vec{l}}_z \end{pmatrix} = \begin{pmatrix} \mathbf{0}_{2x3} & \mathbf{0}_{2x1} & \mathbf{I}_2 & \mathbf{0}_{2x4} & \mathbf{0}_{2x4} \\ & \mathbf{A}_{4x\dots} & & \mathbf{B}_{w,4x\dots} & \\ \mathbf{0}_{4x3} & \mathbf{T}_G^T & & \mathbf{0}_{4x4} & -\mathbf{I}_4 \end{pmatrix} \begin{pmatrix} \vec{\underline{x}} \\ \vec{\underline{w}} \end{pmatrix}
$$

$$
+ \begin{pmatrix} \mathbf{0}_{2x4} \\ \boldsymbol{B}_{u,4x\dots} \\ \mathbf{0}_{4x4} \end{pmatrix} \vec{\underline{u}} \qquad (23)
$$

The geometry matrix $\boldsymbol{T}_G$ was defined in (2). The notation $\bullet_{4x\dots}$ denotes the elements of the fourth row of the matrix $\bullet$. The process noise of the four states $\underline{\dot{z}}_r$ is set high in comparison with the other states, since the dynamic is not known and was set to zero in (21).

The estimated road height profile using this observer drifts, since no high-pass filter is incorporated. This is acceptable, if the frequencies between 0.5 and 5 Hz are estimated with a high degree of precision. Thus, the estimated states $\underline{z}_r$ are forward–backward high-pass filtered to compare the interesting frequencies with the reference profile of Fig. 3(b), which is filtered equivalently. The correlation is known due to a GPS-based system in the vehicle. In Fig. 17, the filtered reference profile and the filtered state of the observer are depicted, they show that the road profile under the wheels can be observed with a high degree of accuracy.

IX. CONCLUSION

Two overall concepts for a preview active suspension control to improve ride comfort over road obstacles are proposed in this study. The first concept consists of generating an inertial-fixed height profile from the measurements of a vehicle body fixed sensor, which is used as input for a MPC; thus, reducing vehicle body accelerations and incorporating constraints on actuator displacement and actuator displacement rate.

For the second approach, a sensor-fixed height profile is generated; thus, changing the orientation of the profile in the coordinate system due to vehicle body motion at each time step. This is eliminated by high-pass forward–backward filtering of the profile at each time step. The resulting height profile under the wheels is used for a feedforward disturbance compensation. The feedforward control is combined with a *Skyhook* feedback controller without preview.

Since low-bandwidth active suspension systems with a bandwidth up to about 5 Hz are considered, only road waves longer as the preview range of the considered sensor can be compensated for by the actuators at high vehicle speeds. Hence, the road wave is not seen entirely at one time step but can still be compensated for with the two proposed concepts, as shown in the simulation results. However, the second concept is preferable for vehicle implementation due to its better modularity, as opposed to an overall optimization and, hence, easier adjustment to all driving situations.

Measurement results are shown for driving over a road obstacle, and an observer is designed to estimate the road profile to verify the signal from the preview sensor. It has been shown that the road profile can be estimated highly accurately with the designed observer and that a major improvement of ride comfort is feasible in vehicle implementation using the proposed algorithms.

REFERENCES

[1] A. G. Thompson, "An active suspension with optimal linear state feedback," *Veh. Syst. Dyn.*, vol. 5, no. 4, pp. 187–203, 1976.

[2] H. Tseng and J. Hedrick, "Semi-active control laws—Optimal and suboptimal," *Veh. Syst. Dyn.*, vol. 23, no. 1, pp. 545–569, 1994.

[3] K. Kim and D. Jeon, "Vibration suppression in an MR fluid damper suspension system," *J. Intell. Mater. Syst. Struct.*, vol. 10, no. 10, pp. 779–786, 1999.

[4] W. Sun, H. Gao, and O. Kaynak, "Finite frequency H$_\infty$ control for vehicle active suspension systems," *IEEE Trans. Control Syst. Technol.*, vol. 19, no. 2, pp. 416–422, Mar. 2011.

[5] A. L. Do, O. Sename, L. Dugard, and B. Soualmi, "Multi-objective optimization by genetic algorithms in H$_\infty$/LPV control of semi-active suspension," presented at the 18th World Congr. Int. Fed. Autom. Control, Milano, Italy, 2011.

[6] J. Wang, D. A. Wilson, and G. D. Halikias, "H$_\infty$ robust-performance control of decoupled active suspension systems based on LMI method," in *Proc. Amer. Control Conf.*, 2001, vol. 4, pp. 2658–2663.

[7] M. C. Smith and F.-C. Wang, "Controller parameterization for disturbance response decoupling: Application to vehicle active suspension control," *IEEE Trans. Control Syst. Technol.*, vol. 10, no. 3, pp. 393–407, May 2002.

[8] M. Fallah, R. Bhat, and W.-F. Xie, "Optimized control of semiactive suspension systems using H$_\infty$ robust control theory and current signal estimation," *IEEE/ASME Trans. Mechatronics*, vol. 17, no. 4, pp. 767–778, Aug. 2012.

[9] W. Sun, H. Gao, and O. Kaynak, "Vibration isolation for active suspensions with performance constraints and actuator saturation," *IEEE/ASME Trans. Mechatronics*, vol. 20, no. 2, pp. 675–683, Apr. 2015.

[10] M. Canale, M. Milanese, and C. Novara, "Semi-active suspension control using 'fast' model-predictive techniques," *IEEE Trans. Control Syst. Technol.*, vol. 14, no. 6, pp. 1034–1046, Nov. 2006.

[11] N. Giorgetti, A. Bemporad, H. Tseng, and D. Hrovat, "Hybrid model predictive control application towards optimal semi-active suspension," in *Proc. IEEE Int. Symp. Ind. Electron.*, Jun. 20–23, 2005, pp. 391–398.

[12] N. Giorgetti, A. Bemporad, H. E. Tseng, and D. Hrovat, "Hybrid model predictive control application towards optimal semi-active suspension," *Int. J. Control*, vol. 79, no. 5, pp. 521–533, 2006.

[13] D. Karnopp, M. Crosby, and R. Harwood, "Vibration control using semi-active force generators," *ASME Trans., J. Eng. Ind.*, vol. 96, pp. 619-626, May 1974.

[14] F. Frühauf, R. Kasper, and J. Lückel, "Design of an active suspension for a passenger vehicle model using input processes with time delays," *Veh. Syst. Dyn.*, vol. 15, pp. 126–138, 1986.

[15] D. Crolla and M. Abdel-Hady, "Active suspension control; performance comparisons using control laws applied to a full vehicle model," *Veh. Syst. Dyn.*, vol. 20, no. 2, pp. 107–120, 1991.

[16] M. Abdel-Hady and D. Crolla, "Active suspension control algorithms for a four-wheel vehicle model," *Int. J. Veh. Des.*, vol. 13, no. 2, pp. 144–158, 1992.

[17] R. Sharp and C. Pilbeam, "On the ride comfort benefits available from road preview with slow-active car suspensions," *Veh. Syst. Dyn.*, vol. 23, pp. 437–448, 1994.

[18] S. EI-Demerdash and D. Crolla, "Hydro-pneumatic slow-active suspension with preview control," *Veh. Syst. Dyn.*, vol. 25, no. 5, pp. 369–386, 1996.

[19] A. Akbari, G. Koch, E. Pellegrini, S. Spirk, and B. Lohmann, "Multi-objective preview control of active vehicle suspensions: Experimental results," in *Proc. 2nd Int. Conf. Adv. Comput. Control*, Mar. 2010, vol. 3, pp. 497–502.

[20] A. Akbari and B. Lohmann, "Output feedback H$_\infty$/GH$_2$ preview control of active vehicle suspensions: A comparison study of LQG preview," *Veh. Syst. Dyn.*, vol. 48, no. 12, pp. 1475–1494, 2010.

[21] N. Louam, D. A. Wilson, and R. S. Sharp, "Optimal control of a vehicle suspension incorporating the time delay between front and rear wheel inputs," *Veh. Syst. Dyn.*, vol. 17, no. 6, pp. 317–336, 1988.

[22] L. Yan and L. Shaojun, "Preview control of an active vehicle suspension system based on a four-degree-of-freedom half-car model," in *Proc. 2nd Int. Conf. Intell. Comput. Technol. Autom.*, 2009, vol. 1, pp. 826–830.

IEEE/ASME TRANSACTIONS ON MECHATRONICS, VOL. 20, NO. 5, OCTOBER 2015

[23] H. S. Roh and Y. Park, "Stochastic optimal preview control of an active vehicle suspension," *J. Sound Vibr.*, vol. 220, no. 2, pp. 313–330, 1999.

[24] M. Tomizuka, "Optimum linear preview control with application to vehicle suspension," *J. Dyn. Syst., Meas. Control*, vol. 98, no. 3, pp. 309–315, 1976.

[25] A. Thompson, B. Davis, and C. Pearce, "An optimal linear active suspension with finite road preview," Society of Automotive Engineers, Inc., Washington, DC, USA, Tech. Paper 800520, 1980.

[26] A. Hac, "Optimal linear preview control of active vehicle suspension," in *Proc. IEEE 29th Conf. Decision Control*, Dec. 1990, vol. 5, pp. 2779–2784.

[27] L. A. Balzer, "Optimal control with partial preview of disturbances and rate penalties and its application to vehicle suspension," *Int. J. Control*, vol. 33, no. 2, pp. 323–345, 1981.

[28] A. Hac, "Optimal linear preview control of active vehicle suspension," *Veh. Syst. Dyn.*, vol. 21, no. 1, pp. 167–195, 1992.

[29] A. Thompson and C. Pearce, "Physically realisable feedback controls for a fully active preview suspension applied to a half-car model," *Veh. Syst. Dyn.*, vol. 30, no. 1, pp. 17–35, 1998.

[30] N. Louam, D. Wilson, and R. Sharp, "Optimization and performance enhancement of active suspensions for automobiles under preview of the road," *Veh. Syst. Dyn.*, vol. 21, no. 1, pp. 39–63, 1992.

[31] I. Youn, " Optimal design of discrete time preview controllers for semiactive and active suspension systems," *KSME Int. J.*, vol. 14, no. 8, pp. 807–815, 2000.

[32] O. Kang, Y. Park, Y.-S. Park, and M. Suh, " Look-ahead preview control application to the high-mobility tracked vehicle model with trailing arms," *J. Mech. Sci. Technol.*, vol. 23, no. 4, pp. 914–917, 2009.

[33] D. Martinus, B. Soenarko, and Y. Nazaruddin, "Optimal control design with preview for semi-active suspension on a half-vehicle model," in *Proc. IEEE 35th Conf. Decision Control*, 1996, vol. 3, pp. 2798–2803.

[34] R. Huisman, F. Veldpaus, H. Voets, and J. Kok, "An optimal continuous time control strategy for active suspensions with preview," *Veh. Syst. Dyn.*, vol. 22, no. 1, pp. 43–55, 1993.

[35] R. Huisman, F. Veldpaus, J. Van Heck, and J. Kok, "Preview estimation and control for (semi-) active suspensions," *Veh. Syst. Dyn.*, vol. 22, nos. 5/6, pp. 335–346, 1993.

[36] J. Marzbanrad, G. Ahmadi, H. Zohoor, and Y. Hojjat, "Stochastic optimal preview control of a vehicle suspension," *J. Sound Vibr.*, vol. 275, nos. 3–5, pp. 973–990, 2004.

[37] S. Senthil and S. Narayanan, "Optimal preview control of a two-DOF vehicle model using stochastic optimal control theory," *Veh. Syst. Dyn.*, vol. 25, pp. 413–430, 1996.

[38] R. Mehra, J. Amin, K. Hedrick, C. Osorio, and S. Gopalasamy, "Active suspension using preview information and model predictive control," in *Proc. IEEE Int. Conf. Control Appl.*, Oct. 1997, pp. 860–865.

[39] B. Cho, "Active suspension controller design using MPC with preview information," *J. Mech. Sci. Technol.*, vol. 13, pp. 168–174, 1999.

[40] B.-K. Cho, G. Ryu, and S. J. Song, "Control strategy of an active suspension for a half car model with preview information," *Int. J. Autom. Technol.*, vol. 6, pp. 243–249, 2005.

[41] C. Göhrle, A. Wagner, A. Schindler, and O. Sawodny, "Active suspension controller using MPC based on a full-car model with preview information," in *Proc. IEEE Amer. Control Conf.*, Jun. 27–29, 2012, pp. 497–502.

[42] C. Göhrle, A. Schindler, A. Wagner, and O. Sawodny, "Model predictive control of semi-active and active suspension systems with available road preview," in *Proc. IEEE Eur. Control Conf.*, 2013, pp. 1499–1504.

[43] C. Göhrle, A. Schindler, A. Wagner, and O. Sawodny, "Design and vehicle implementation of preview active suspension controllers," *IEEE Trans. Control Syst. Technol.*, vol. 22, no. 3, pp. 1135–1142, May 2014.

[44] A. Unger, F. Schimmack, B. Lohmann, and R. Schwarz, "Application of LQ based semi-active suspension control in a vehicle," presented at the 18th World Congr. Int. Fed. Autom. Control, Milano, Italy, Aug. 28–Sep. 2, 2011.

[45] D. Hrovat, "Survey of advanced suspension developments and related optimal control applications," *Automatica*, vol. 33, no. 10, pp. 1781–1817, 1997.

[46] R. A. Fisher, "On an absolute criterion for fitting frequency curves," *Messenger Math.*, vol. 41, pp. 155–160, 1912.

[47] J. Aldrich, "R.A. fisher and the making of maximum likelihood 1912–1922," *Statist. Sci.*, vol. 12, no. 3, pp. 162–176, 1997.

[48] G. Welch, and G. Bishop, "An introduction to the Kalman filter," Dept. Comput. Sci., University of North Carolina at Chapel Hill, Chapel Hill, NC, USA, Tech. Rep. TR 95-041, Jul. 2006.

[49] A. Schindler, "Neue Konzeption und erstmalige Realisierung eines aktiven Fahrwerks mit Preview-Strategie," Ph.D. dissertation, Institute for Applied Computer Science, Karlsruher Institut für Technologie, Karlsruher, Germany, 2009.

[50] A. V. Oppenheim and A. S. Willsky, *Signale und Systeme*. New York, NY, USA: VCH, 1989.

[51] F. Gustafsson, "Determining the initial states in forward-backward filtering," *IEEE Trans. Signal Process.*, vol. 44, no. 4, pp. 988–992, Apr. 1996.

Christoph Göhrle was born in Marktoberdorf, Germany. He received the Dipl.Ing. degree in mechanical engineering from the Technische Universität München, Munich, Germany, in 2010. Since 2011, he has been working toward the Ph.D. degree at the Institute for System Dynamics, University of Stuttgart, Stuttgart, Germany.

He has been a Research Engineer at the University of Stuttgart. His current research interests include active and semiactive suspension systems, model predictive control, as well as industrial applications with emphasis on preview active suspension control.

Andreas Schindler received the Dipl.Ing. degree in mechanical engineering from the University of Karlsruhe, Karlsruhe, Germany, in 2002, and the Ph.D. degree from the Karlsruhe Institute of Technology, Karlsruhe, Germany, in 2009.

In 2007, he joined the Advanced Chassis Engineering Department, AUDI AG, Ingolstadt, Germany, where he has been involved in the field of control design for active suspension systems. His current research interests include methods of preview control for active suspensions and applications to mechatronics suspension systems.

Andreas Wagner received the Dipl.Ing. degree in mechanical engineering from the University of Applied Sciences, Ulm, Germany, in 1999, and the Ph.D. degree from the University of Stuttgart, Stuttgart, Germany, in 2003.

He joined the Department of "Aerodynamics & Aeroacoustics," Audi, Ingolstadt, Germany, in 2003, and became a Manager of the Department of "Development of HVAC-Systems" in 2008. Since 2010, he has been responsible for the development of "vehicle attributes of chassis concepts."

Oliver Sawodny received the Dipl.Ing. degree in electrical engineering from the University of Karlsruhe, Karlsruhe, Germany, in 1991, and the Ph.D. degree from the University of Ulm, Ulm, Germany, in 1996.

In 2002, he became a Full Professor at the Technical University of Ilmenau, Ilmenau, Germany. Since 2005, he has been the Director of the Institute for System Dynamics, University of Stuttgart, Stuttgart, Germany. His current research interests include methods of differential geometry, trajectory generation, and applications to mechatronic systems.

Authorized licensed use limited to: TONGJI UNIVERSITY. Downloaded on November 03,2025 at 10:49:25 UTC from IEEE Xplore. Restrictions apply.